National Conference with International Participation

ENGINEERING MECHANICS 2008

Svratka, Czech Republic, May 12 – 15, 2008

EXPERIMENTAL AND NUMERICAL MODELLING OF TURBULENT FLOW OVER TRANSVERSAL RIBS IN AN OPEN CHANNEL

J. Příhoda*, J. Šulc, M. Sedlář***, P. Zubík****

Summary: Modelling of turbulent flow in an open channel with transversal ribs on its bottom was concentrated particularly on the development of flow separation behind ribs and on the corresponding changes of free surface. Further, the pressure drag of individual ribs was investigated including their dependence on the rib spacing, as well as the origin of secondary flow near the side walls of the channel behind ribs. Numerical results obtained by the software ANSYS CFX 11.0 were compared with experiments carried out by means of LDA and PIV techniques in free-surface water channel 200x200 mm with one and/or two transversal ribs 10xl0 mm with various spacing.

1. Introduction

Wall roughness considerably influences flows in nearly all engineering and environmental applications. Wall roughness increases friction losses on one hand but on the other hand intensifies momentum and heat transfer. Besides distributed wall roughness given by manufacturing technique (concrete walls) and/or by the influence of operating conditions (corrosion, erosion), rough surface is often formed by obstacles on channel walls for intensification of heat transfer e.g. in cooling channels of gas turbine blades or for retardation of water discharged from impounding reservoirs.

Turbulent flow in open channels with transversal ribs on its bottom was investigated by Chára and Hoření (2006) and Tachie and Adane (2007) but in both cases for subcritical flow conditions only. This contribution deals with the experimental and numerical modelling of supercritical flow over one and/or two transversal ribs on the bottom of an open channel. A part of experimental results was published by Šulc et al. (2006) and Zubík (2007). Some preliminary simulations using software FLUENT have been made by Sládek and Příhoda (2007) and by Sládek et al. (2007).

* Prof. Ing. Jaromír Příhoda, CSc., Institute of Thermomechanics, v.v.i., AS CR, Dolejškova 5, 182 00 Praha 8; phone: +420 266 053 824, fax: +420 286 584 695, e-mail: prihoda@it.cas.cz

** Prof. Ing. Jan Šulc, CSc., Ing. Pavel Zubík, PhD., Institute of Hydraulic Structures, Faculty of Civil Engineering, University of Technology, Veveří 331/95, 602 00 Brno; phone: +420 541 147 286; fax: +420 541 147 288; e-mail: Sulc.J@fce.vutbr.cz, Zubik.P@fce.vutbr.cz

*** Ing. Milan Sedlář, CSc., SIGMA – Research and Development Institute, Jana Sigmunda 79, 783 50 Lutín; phone: +420 585 652 423, fax: +420 585 652 400, e-mail: milan.sedlar@sigma-vvu.cz

2. Experimental arrangement

The test apparatus for the experimental investigation of turbulent flow in an open channel with ribs was formed by a straight channel of constant cross-section 0.2×0.2 m with the length 4.475 m and with the slope of the bottom 4.77 %. The overall view of the water channel is given in Fig.1. The channel was made of transparent plastic material allowing the use of contactless optical measuring techniques. To stabilize the inflow rate, a wire mesh screens and a honeycomb were installed at the entry of the straight inflow part. One and/or two transversal ribs of the square cross-section b×b = 10×10 mm were placed at the channel bottom with spacing t = 60; 100 and 200 mm. The distance of the first rib from the channel entry was 1.165 m.

Fig.1 Overall view of the water channel with ribs

Two contactless optical methods for velocity field measurement have been used - the plane laser anemometry (Particle Image Velocimetry) for measurements of the velocity field in selected channel sections, and the point laser anemometry (Laser Doppler Anemometry) for measurements of one and/or two velocity components in selected points of the flow field. The measurement of the overcritical flow was carried out for the mean bulk velocity U_m = 2.3 m/s and for the initial height of the water level h = 46 mm, i.e. for the Reynolds number $Re_b = U_m b/\nu$ = 25500 and the Froudé number $Fr = U_m/(gh)^{1/2}$ = 3.42.

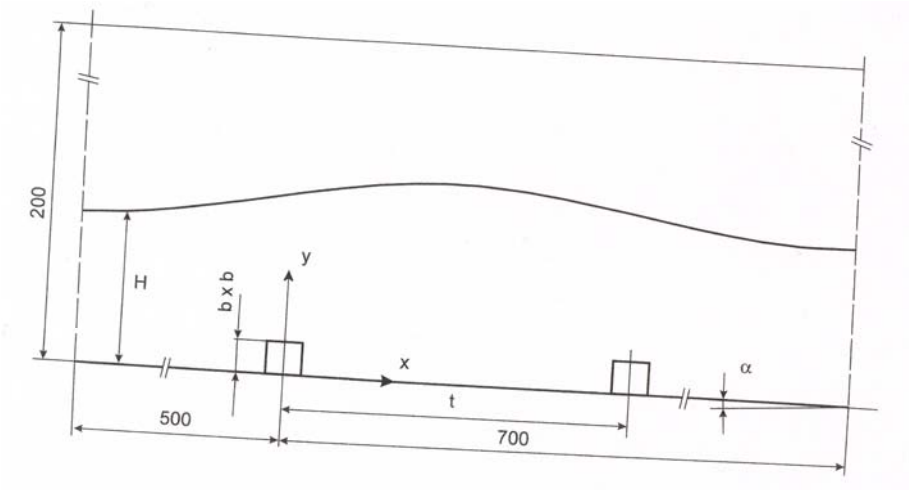

Fig.2 Sketch of the geometrical arrangement of the channel with two ribs

The sketch of the geometrical arrangement is shown in Fig.2. The whole length of the investigated section was 1.2 m. This section starts in the distance of 0.5 m before the first rib where boundary conditions for the numerical simulation were examined in detail using the PIV method. In this section, velocity profiles were recorded using the LDA method as well. At the chosen mean bulk velocity, the turbulence level in the stream core was about 2-2.5 %. The PIV measurements were taken at vertical and horizontal planes parallel with the channel axis with the aim to determine the general view of the flow with separation and secondary flows behind the first rib as well. In the mean vertical plane, profiles of mean and fluctuation longitudinal velocities were determined by the LDA method at selected sections x = const.

3. Numerical simulation

The numerical simulation of the supercritical flow over ribs in an open channel was carried out by means of the commercial software ANSYS CFX 11.0 solving Reynolds-averaged Navier-Stokes equations including the gravity effect. The Volume-of-Fluid (VOF) method was used for the solution of free-surface flow. The VOF method is based on the monitoring of the volume fraction α_i of both fluids in the each computational cell. The free surface is determined as the interface where $\alpha_{water} = \alpha_{air} = 0.5$ is valid.

The two-equation turbulence models - especially standard k-ε turbulence model and the k-ε/k-ω SST model according to Menter (1994) taking into account the turbulent shear stress transport - were tested, particularly their ability to describe the separation region behind ribs and the form of the free surface. Secondary flow in horizontal planes behind the rib near the side wall of the channel was followed as well.

A second-order scheme was used for calculations. The scheme reduced to the first order near discontinuities of the boundary. The computational domain constitutes one half of the channel width, i.e. the symmetrical boundary condition is applied in the symmetry plane (z=0).

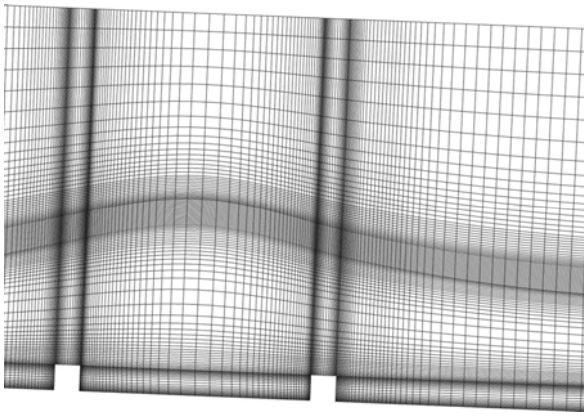

Fig.3 Detail of the computational grid for the channel with two ribs

A structured multi-block type grid refined near walls and in the region of free surface was used. The detail of the computational grid for the channel with two ribs is shown in Fig.3. The computational grid consists of 3 or 4 blocks for case of 1 or 2 ribs respectively and includes about $1\text{-}1.25\times10^6$ grid points depending on the spacing of ribs. For each configuration of ribs, the topology and refinement of the grid were adapted to the shape of free surface obtained by the first preliminary calculation. Values of first non-dimensional distance y^+ from the bottom and ribs moved from 0.5 to 24.

While the k-ε model uses standard wall functions, boundary conditions at the wall in the SST model are prescribed depending on the mesh density either in form of wall functions or by automatic switch to the low-Reynolds-number formulation, see Grotjans and Menter (1998). The distribution of mean velocity, turbulent energy, and dissipation rate was prescribed as inflow boundary conditions according to experimental data. According to value of the Froudé number, the mean value of static pressure was prescribed as the outflow boundary condition (so called supercritical boundary condition). The open-boundary condition was applied at the upper boundary.

4. Results

The analysis of the experimental and numerical results was concentrated mainly on the development of flow separation behind ribs and on the corresponding changes of free surface. Further, the pressure drag of individual ribs was investigated including their dependence on the rib spacing, as well as the origin of secondary flow near the side walls of the channel behind ribs.

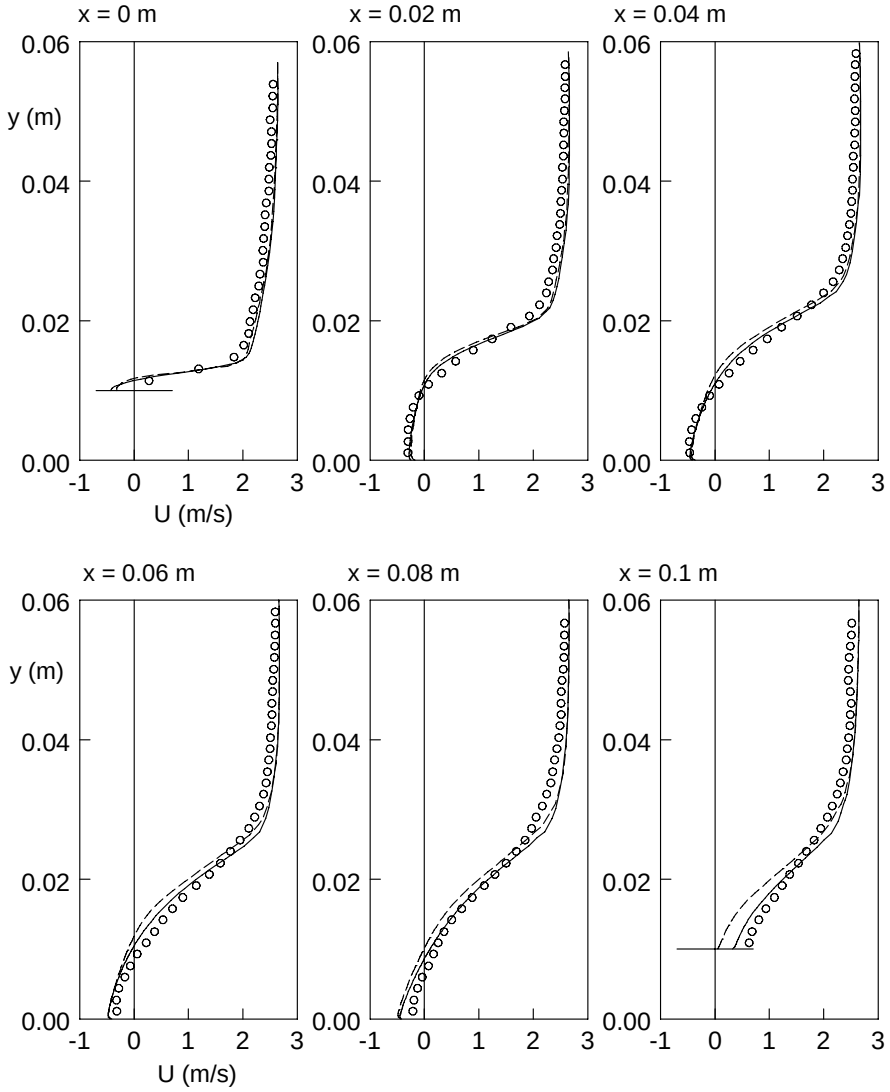

Fig.4 Mean velocity profiles in the channel with two ribs and spacing t = 100 mm (full line – k-ε model; dashed line – SST model)

Fig.4 shows mean velocity profiles in the symmetry plane for two ribs with spacing t = 100 mm. Velocity profiles obtained by means of the k-ε model (full line) and by the SST model (dashed line) are compared with experimental data from PIV technique. The agreement of calculated and measured velocity profiles is quite good. The predicted relaxation of the separated shear layer behind the rib is rather slower and so the numerical simulation gives a greater extent of the separation region. The difference between mean velocities measured by the LDA a PIV technique is really small in regions of attached flow but the LDA technique gives in the separated flow mean velocities slightly higher – the difference reaches up to 10%. The k-ε model gives surprisingly better results than the SST model which was however proposed to refine the prediction of decelerating flows with possible separation due to adverse pressure gradient.

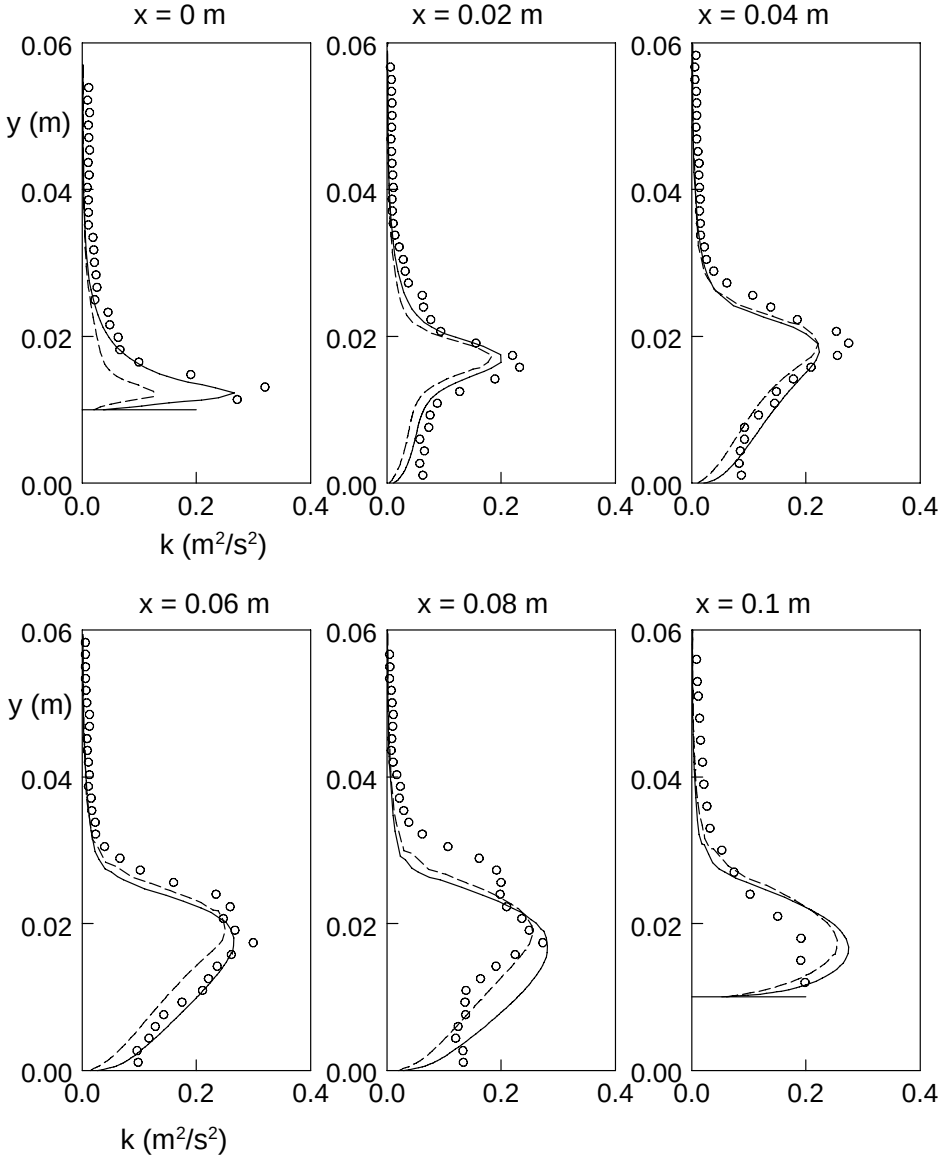

Fig.5 Profiles of turbulent energy k and longitudinal velocity fluctuation $\overline{u^2}$ in the channel with two ribs and spacing t = 100 mm (full line - k-ε model; dashed line - SST model)

The flow separation at the upper wall of the first rib extends practically to the second rib for spacing t = 60 and 100 mm. The length of the separated region behind first rib is approximately x/b ~ 8 for t = 200 mm and corresponds to the separation behind the backward facing step. Simultaneously, a sharp increase of the free surface occurs due to presence of ribs. The extent of the separation region behind the second rib is much shorter and it is influenced by the "forcing" effect of the free surface returning gradually into the initial state.

Profiles of turbulent energy k determined by means of k-ε model and the SST model in the middle plane of the channel are compared in Fig.5 with profiles of longitudinal velocity fluctuations $\overline{u^2}$ achieved by the one-component PIV measurement. Although the direct comparison of longitudinal velocity fluctuation and turbulent energy is not possible, the accordance of measured and computed position of the maximum of turbulent energy is very well apparent. A sharp increase of turbulent energy occurs at the separation with a maximum at the upper boundary of reverse flow. Further downstream the first rib, the maximum of turbulent energy lies in the outer shear flow. An illustrative picture of the turbulent energy distribution in the middle plane of the channel between both ribs is given in Fig.6 for various spacing of ribs. Numerical results were obtained using the k-ε model.

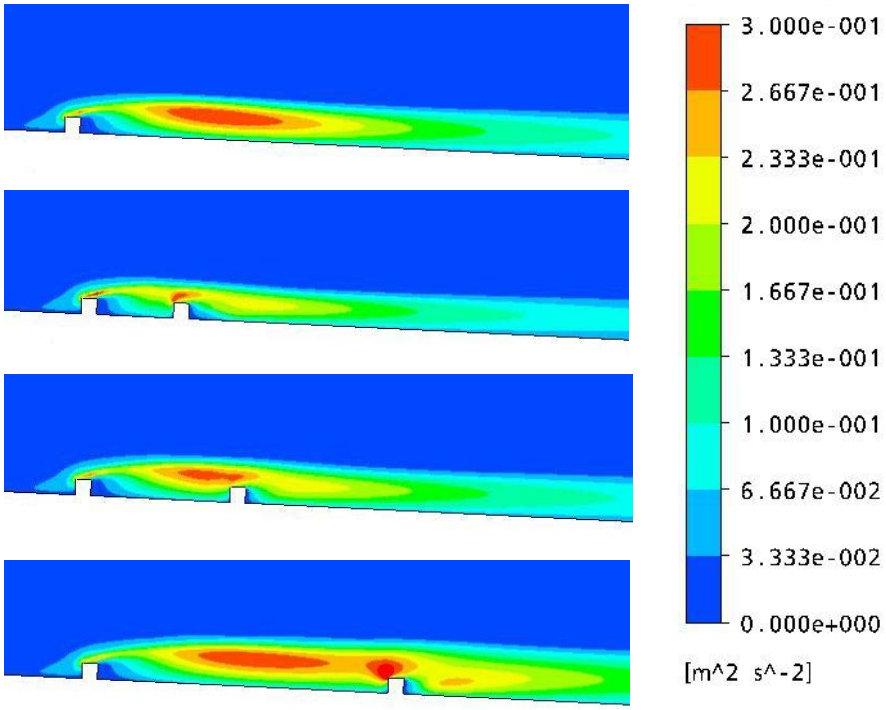

Fig.6 Distribution of turbulent energy in the middle plane of the channel
a) one rib; b) two ribs, t = 60 mm; c) two ribs, t = 100 mm; d) two ribs, t = 200 mm

The form of the free surface in the channel with one rib is shown in Fig.7a. The picture was obtained as the mean value of 50 images. The free surface obtained by numerical simulation is given in Fig.7b as the distribution of the volume fraction of water $\alpha_{water} = 0.5$ in the symmetry plane of the channel. Results of the k-ε model are shown by the full line while the ones of the SST model by the dashed line. Experimental results are shown by dotted lines. Further, the extent of separation region behind the rib obtained by experiment and by numerical simulation is compared in Fig.7b as well.

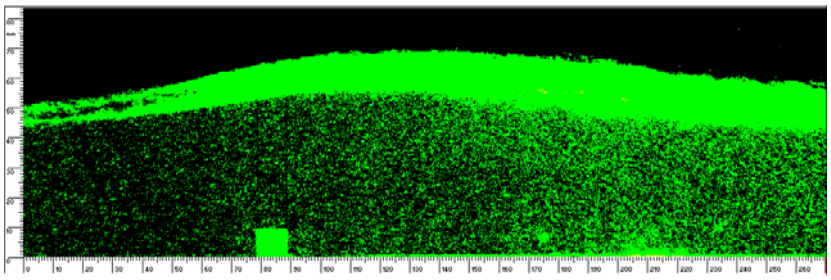

a) experiment

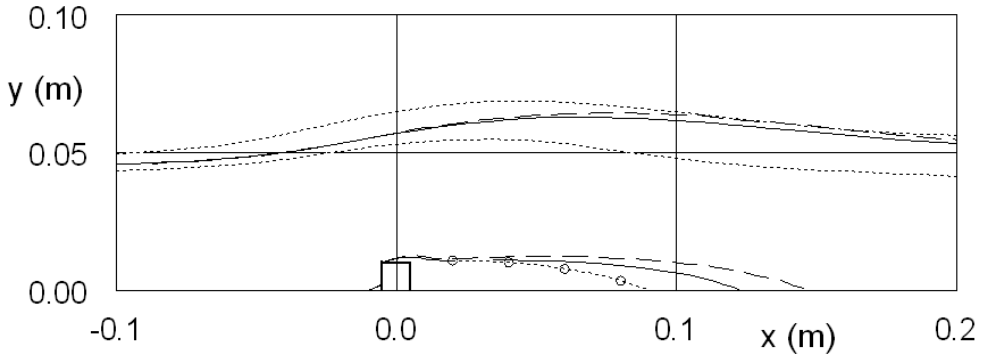

b) comparison with numerical simulation

Fig.7 Flow in the open channel with one rib

The form of free surface in the channel with two ribs and spacing t = 100 mm is shown in Fig.8. Identically as in Fig.7, numerical results are compared with experimental data obtained as the mean value of 50 images. Numerical simulation gives a smaller rise of free surface over the first rib and a slower return to the free surface of the non-disturbed flow behind the second rib. It follows from the slower relaxation of fluid flow in numerical simulation, as it can be seen from profiles of longitudinal mean velocity and velocity fluctuation given in Figs.4 and 5.

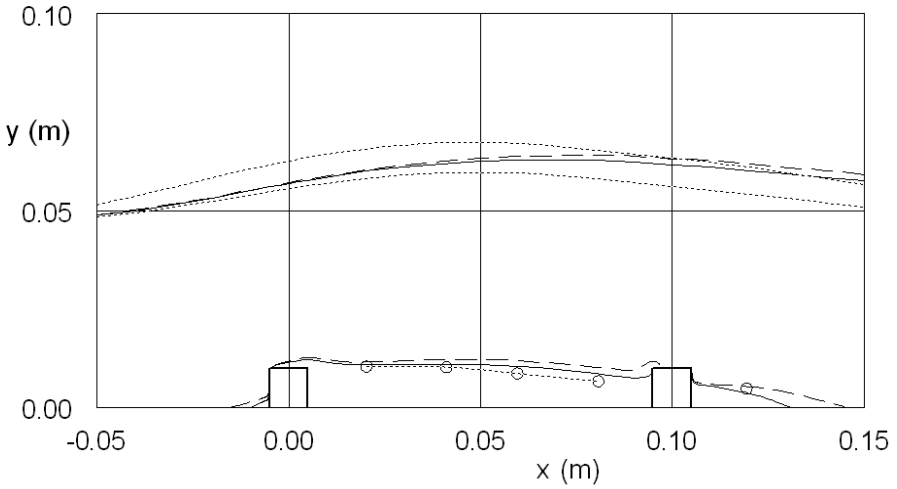

Obr.8 Flow in the open channel with two ribs

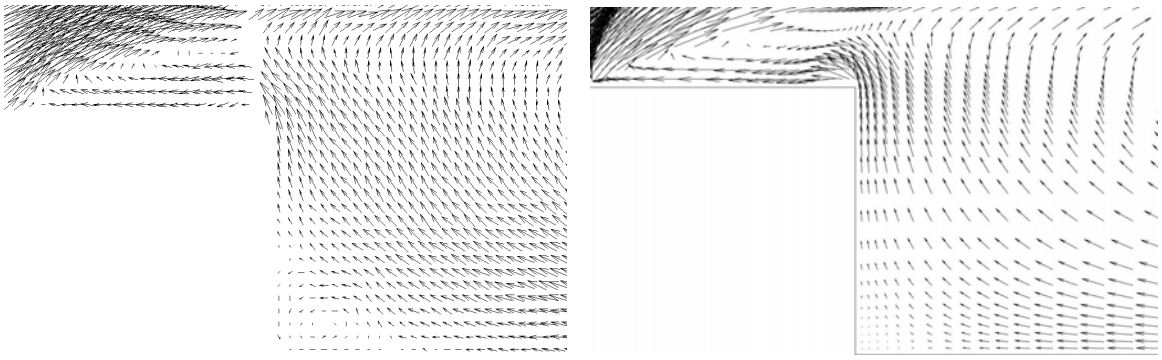

a) PIV measurement b) numerical simulation (SST model)

Fig.9 Detail of mean velocity field behind the first rib in the middle plane of the channel with two ribs and spacing t = 60 mm

The detail of the mean velocity field behind the first rib is given in Fig.9 for the channel with two ribs and spacing t = 60 mm. A small secondary vortex can be seen near the bottom just behind the rib. This vortex is better visible in numerical simulation by means of the SST model than by the k-ε model. Surprisingly, the intensity of this vortex is not constant across the width of the channel. The maximum intensity of the vortex is approximately in one-fourth of the channel width.

Mean velocity field between ribs in the plane parallel to the channel bottom at the height y = 2 mm above the bottom is shown in Fig.10. Because of the chosen computational domain, the picture shows one half of the channel width. The secondary vortex behind the rib near the channel side wall is well apparent in experimental and numerical results as well. The SST model gives a somewhat more noticeable secondary movement than the k-ε model. The similar vortex can be seen behind the backward facing step. According to experimental results the vortex structure behind the rib is more complex because four vortices can been recognised across the channel near the rib.

channel axis

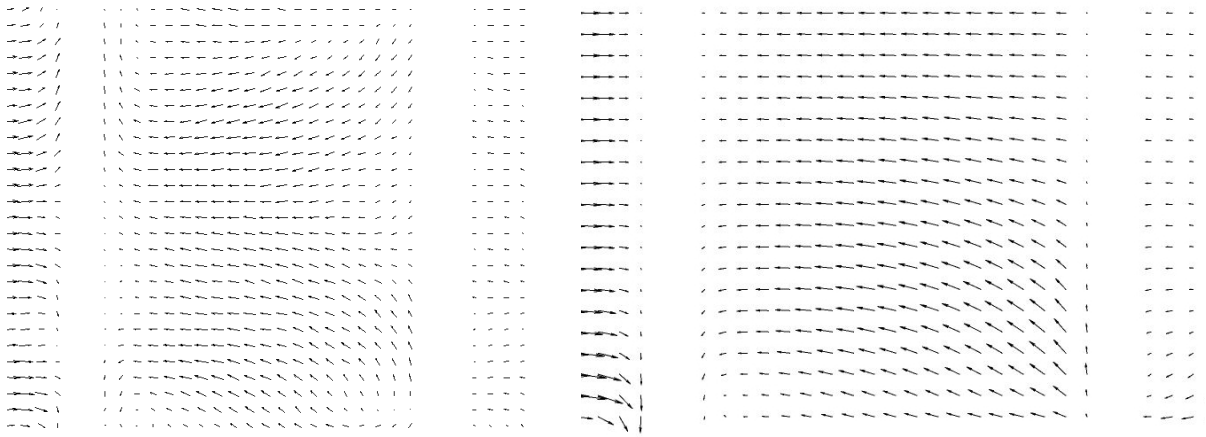

side wall

a) PIV measurement b) numerical simulation (k- ε model)

Fig.10 Mean velocity vectors in the plane 2 mm above the channel bottom (t = 100 mm)

Further, the drag of individual ribs given by the pressure difference on the front and back side of a rib was determined from numerical simulations. The drag coefficient is given by the relation $c_d = 2\Delta p/\rho U_m^2$ where Δp is the mean value of the pressure difference on the front and back side of a rib and U_m is the bulk velocity. The dependence of the drag coefficient c_d of both ribs on their spacing is given in Fig.11. For small spacing, the second rib lies in the wake of the first one and the pressure force can be oriented upstream. The drag of both ribs approaches the value determined for flow with one rib (dotted lines).

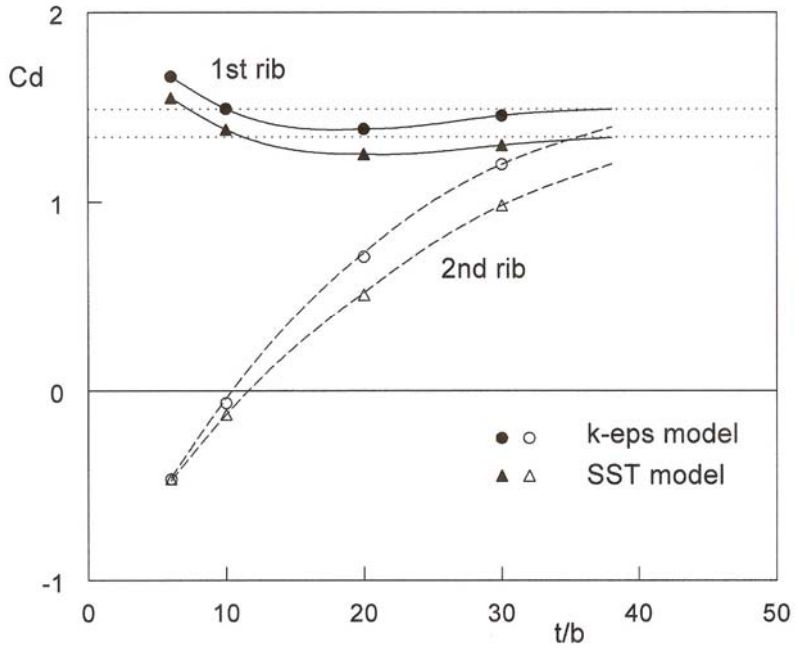

Fig.11 Variation of the drag coefficient with rib spacing

5. Conclusions

The analysis of the supercritical flow in an open channel with ribs on its bottom was concentrated mainly on the development of flow separation behind ribs and on the corresponding changes of free surface. Further, the pressure drag of individual ribs was investigated including their dependence on the rib spacing, as well as the origin of secondary flow near the side walls of the channel behind ribs.

The numerical simulation of the supercritical flow over one and/or two transversal ribs carried out by means of the commercial software ANSYS CFX 11.0 gives a quite good agreement with experimental data. An acceptable agreement of mean velocity and turbulent characteristic was achieved using two-equation turbulence models, even though the numerical simulation gives a smaller rise of free surface over the first rib and a slower return to the free surface of the non-disturbed flow behind the second rib. The common lack of two-equation turbulence models is a slow relaxation of shear layer after separation. It results in the greater extent of the separation region with an adequate form of predicted free surface.

Numerical results allowed the estimation of the effect of the rib arrangement on the pressure drag of ribs. The dependence of the pressure drag on the rib spacing can be used for the optimal arrangement of ribs used for the retardation of water discharged from impounding reservoirs.

Acknowledgement

The work was supported by the grant project No.103/06/0461 of the Czech Science Foundation and by the Research Plan AV0Z20760514.

References

Chára Z., Hoření B. (2006): Local resistance of surface mounted obstacles, Proc. Conf. Engineering Mechanics 2006 (Ed. Náprstek J., Fischer C.), Svratka, 126-127, CR ROM, 9 p.

Grotjans H., Menter F. (1998): Wall functions for general application CFD codes, Proc. ECCOMAS 98, John Wiley & Sons, 1998, 1112-1117

Hoření B., Chára Z. (2004): Experimental and numerical modelling of flow around the obstacles placed on a channel bottom, Proc. Conf. Engineering Mechanics 2004 (Ed. Zolotarev I., Poživilová A.), Svratka, 113-114, CD ROM, 12 p.

Menter F.R. (1994): Two-equation eddy-viscosity turbulence models for engineering applications, AIAA J., 32, 1598-1605

Sládek A., Příhoda J. (2007): Modelling of flow over one transversal rib in a channel with free surface, Proc. Conf. Topical Problems of Fluid Mechanics, Praha, 157-160 (in Czech)

Sládek A., Příhoda J., Stanislav J. (2007): Modelling of flow over two transversal ribs in a channel with free surface, Proc. Colloquium Fluid Dynamics, Praha, 81-82, CD-ROM, 8 p. (in Czech)

Šulc J., Zubík P., Žoužela M. (2006): Measurement of parameters of supercritical flow in a channel with transversal ribs on the bottom, Proc. Conf. Hydrodynamics 2006, Rajnochovice, 134-139 (in Czech)

Tachie M.F., Adane K.K. (2007): PIV study of shallow open channel flow over d- and k-type transverse ribs, Trans ASME, J. Fluids Eng., 129, 1058-1072

Zubík P. (2007): LDA and PIV measurement of flow parameters in a channel with transversal ribs on the bottom, Proc. Conf. Topical Problems of Fluid Mechanics, Praha, 199-202 (in Czech)